Chemical Engineering Journal xxx (2012) xxx–xxx

Contents lists available at SciVerse ScienceDirect

Chemical Engineering Journal

journal homepage: www.elsevier.com/locate/cej

A multi-component two-phase lattice Boltzmann method applied to a 1-D Fischer–Tropsch reactor

M.R. Kamali [a,*], S. Sundaresan [a,b], H.E.A. Van den Akker [a], J.J.J. Gillissen [a]

[a] Department of Multi-Scale Physics, Delft University of Technology, Delft, Netherlands
[b] Department of Chemical Engineering, Princeton University, Princeton, NJ, USA

HIGHLIGHTS

- A multi-component two-phase catalytic reaction was modelled with the lattice Boltzmann method.
- A model was proposed and validated for liquefaction due to the first order surface reaction.
- A relation for surface reaction constant implementation in the modified bounce-back rule was proposed.
- Transient of syngas ratio, liquid film growth, selectivity and paraffin product distribution in a 1-D FTS reactor was calculated.

ARTICLE INFO

Article history:
Available online xxxx

Keywords:
Lattice Boltzmann
Fischer–Tropsch
Multi-component two-phase
Surface reaction
Phase change

ABSTRACT

A multi-component two-phase lattice Boltzmann method of the Shan–Chen type has been developed for simulating the complex interplay of diffusion and surface reaction in a multi-component gas–liquid catalytic chemical reactor. This method development comprised of various steps, viz. the formulation, implementation, and validation of lattice Boltzmann techniques capable of reproducing, among other things, species transport across a phase interface, a chemical reaction at a catalytic surface, and a phase change due to the surface reaction, which all are relevant to the Fischer–Tropsch Synthesis (FTS). The most important steps taken in developing method and implementation, along with some validations are discussed. This paper presents the results of the simulations for a simplified isothermal 1-D FTS case with a liquid film covering a catalytic surface and gradually growing due to the surface reaction.

1. Introduction

Multi-component two-phase catalytic reactors are widely used in refineries, petrochemical plants, pharmaceutical processes, and so on. Despite their widespread application, the complex and dynamic interplay between the various sub-processes involved in this type of reactors generally is not well understood. Computational Fluid Dynamics (CFDs) methods may be useful for increasing our understanding of all interactions involved, provided they zoom in onto the micro- and meso-scales. Such an increased understanding may be helpful in optimising the design of these reactors and their operation.

The complex interaction of two-phase flow, interface positions, species and heat transport, and chemical reactions including phase transition is described by a large set of non-linear partial differential equations. Solving this set of equations with the common Finite Volume (FV) techniques is a very tedious job that even dedicated CFD codes have great difficulty with [1]. Lattice Boltzmann (LB) techniques seem to provide an attractive alternative.

As far as single-phase laminar and turbulent fluid flows are concerned, LB methods have successfully been exploited both for Direct Numerical Simulations (in which all velocity scales are resolved) [2,3] and for Large Eddy Simulations (which make use of sub-grid scale modelling for the smaller motions) [4]. In such simulations, LB is much faster than FV [2]. LB methods have also successfully been applied for analysing bubbly flows and particle suspensions [5–7]. With multiple phases, LB methods do not necessarily need tracking of the many phase interfaces such as done with the volume of fluid or level set techniques in the traditional FV approaches. In fact, in several implementations of the LB method, e.g., the Shan–Chen approach [8], phase separation is an automatic outcome of the algorithm that computes density variations. This also substantially simplifies the numerical simulation of interfacial mass transport [1].

In dealing with species diffusion problems, the LB approach is third order accurate [9]. The kinetic nature of the method allows us to effectively incorporate chemical reactions both at catalytic surfaces and in the bulk of the flow [10,11]. Last but not least,

* Corresponding author. Tel.: +31 (0)15 27 83252; fax: +31 (0)15 27 82838.
E-mail addresses: m.r.kamali@tudelft.nl, mdrzkamali@gmail.com (M.R. Kamali).

1385-8947/$ - see front matter © 2012 Elsevier B.V. All rights reserved.
http://dx.doi.org/10.1016/j.cej.2012.07.019

the method offers the possibility of including complex and irregular solid boundaries which could act as catalytic surfaces as well [12–14].

LB based techniques, however, also struggle with shortcomings which still hinder their broad application. A particularly relevant issue is related to so-called parasitic currents at curved interfaces [1,15]. These unphysical velocities might create inaccuracies in evaluating species transport across the phase interfaces. The parasitic currents, which so far have been intrinsic to the LB method [16], might get intensified in the case of larger density ratios between multiple components or phases. Numerical techniques aimed at mitigating these unphysical velocities have been proposed [15,17].

In general, using LB techniques requires a translation from the conventional continuum variables (velocities, concentration, viscosity, diffusivity, etc.) into typical LB variables. For tuning these LB variables such as to reproduce the continuum variables, one needs quite some expertise and delicacy, particularly in the case of a large number of components and phases which involve many mutual interactions. Of course, also numerical stability issues play a role in LB, just like in FV techniques. Yet, LB techniques look very attractive for the purpose of a detailed investigation of the mutual interaction of two-phase flow, mass and heat transport, and chemical reactions.

This paper reports on the development and application of a LB based technique to be used for simulating multi-component multi-phase (gas–liquid–solid) heterogeneous reactions. The focus is on the Fischer–Tropsch Synthesis (FTS) as an example of an industrially important process. In the FTS, the gaseous reactants of the syngas (carbon monoxide and hydrogen) are converted into liquid hydrocarbons (mainly paraffins) and water with the help of a catalyst. The stoichiometric formulation of the reaction is as follows:

$$n\mathrm{CO} + (2n+1)\mathrm{H_2} \rightarrow \mathrm{C}_n\mathrm{H}_{2n+2} + n\mathrm{H_2O} \quad (1)$$

Some of the aspects at stake are the mass transfer of multiple components in mixtures across a phase interface as well as the interplay between a surface reaction and the associated formation of liquid that limits the supply of fresh gaseous species and the removal of water vapour. For the time being, heat transport has been ignored; it will be the subject of a separate paper.

Our method exploits the pseudo-potential multi-component multi-phase LB model due to Shan and Chen [8] modified to include more realistic equations of state – see [18] – in order to deal with the phase density ratios of current interest which are around 30. The Shan–Chen method is capable of dealing with multi-component convection–diffusion problems [19,20]. In order to incorporate the surface reaction, a bounce-back rule – the usual LB technique for mimicking the no-slip boundary condition in flow simulations [21] – was applied [11,12,22].

This paper is about applying an LB approach for simulating the essentials of the FTS. First, the kinetics of the FTS reaction as used in our LB simulations is described. Then, some aspects of our LB approach relevant for the FTS case study are highlighted. The core of the paper is the implementation of the surface reaction in our LB code and the validation of the code for both single-phase and two-phase surface reactions by means of analytical solutions. Finally, we present simulation results of applying the developed LB code for the case of an isothermal 1-D FTS reaction involving a multi-component chemical reaction with phase change at a catalytic surface.

2. Kinetics of the FTS

The FTS involves the reaction of synthesis gas components (CO, H_2) on the active sites of a catalyst surface resulting in the formation of liquid paraffins and water vapour, given the usual operating conditions. For the gaseous reactants, access to the active sites of the catalyst requires two consecutive conceptual steps which usually are described in terms of external and internal mass transfer limitations, respectively. In the first step, the gaseous components have to diffuse through a liquid layer that fully wets the catalyst surface and which could be either product components or a liquid injected for heat transfer purposes. In the second step, the reactants need to diffuse into the porous structure of the catalyst to find access to the active sites of the catalyst which leads to internal mass transfer limitations. The paraffin products and the water have to diffuse back towards the gas–liquid interface while overcoming similar internal and external mass transfer resistances.

For the kinetics of the FTS, different models are available in the literature. These models should consider the above transport limitations for both reactants which affect selectivity and reactivity. Usually, the FTS is conceived as a polymerisation type of reaction, in which the monomers produced on the surface of the catalyst are added stepwise to a growing aliphatic chain. The result is a mixture of hydrocarbons with a certain chain length distribution. The eventual product distribution in the FTS comes about by a dynamic balance between chain growth and chain termination probabilities as described by the Anderson–Schulz–Flory (ASF) model [23–25].

In this ASF model, the chain growth probability α is defined as $\alpha = r_P/(r_P + r_T)$, where r_P denotes chain growth rate [mole/mass − cat · time] and r_T is the chain termination rate. The chain length distribution of the paraffinic product $\mathrm{C}_n\mathrm{H}_{2n+2}$ is represented by either the mass fraction x_n or the mole fraction χ_n defined by

$$x_n = n(1-\alpha)^2\alpha^{n-1}; \quad \chi_n = (1-\alpha)\alpha^{n-1} \quad (2)$$

Chain growth probability α does not depend on carbon chain length, at least for chains with more than 2 carbon numbers [23]. It does depend, however, on catalyst type, temperature, and H_2/CO or syngas molar ratio [25] as shown in

$$\alpha = \frac{1}{1 + \kappa_\alpha \left(\frac{[\mathrm{H_2}]}{[\mathrm{CO}]}\right)^{\beta} \exp\left(\frac{-\Delta E_\alpha}{R}\left(\frac{1}{493.15} - \frac{1}{T}\right)\right)} \quad (3)$$

in which κ_α denotes the ratio of the rate constants for the propagation and termination reactions; $[H_2]/[CO]$ is the syngas molar concentration ratio; β is an empirical exponent; ΔE_α [J/mole] is the difference between the activation energies of the propagation and termination reactions; R denotes the gas constant and T [K] is temperature. According to this equation, α approaches zero when syngas ratio and temperature increase, and it approaches unity when they decrease.

Zimmerman et al. [26] was the first to report on the diffusion limitation of H_2 in iron-based catalyst particles with a diameter larger than 0.2 mm. Therefore, it is sufficiently accurate to use a kinetics model which is first order with respect to H_2 and zero order with respect to CO. Later on, Post et al. [27] found the same dependence for some iron-based and cobalt-based catalysts at high temperatures ($T > 500$ K). This approximation is only valid, however, for CO conversions up to 60% [28,29]; for CO conversions beyond 60%, also CO will become a limiting component rendering the reaction rate first order with respect to CO. More complicated and more accurate kinetic models are available for the FTS, such as that due to Yates and Satterfield [30]. In our case study, we used the Post et al. kinetics for the sake of its simplicity and reasonable accuracy.

According to the Post et al. model and under the above restriction on CO conversion, the molar stoichiometric reaction rates r [mole/(length^2 time)] for all components in terms of their molar concentrations may be written as

$$r_{\mathrm{CO}} = -r_{\mathrm{H_2O}} = -k_s[\mathrm{H_2}], \quad r_{\mathrm{H_2}} = \frac{2n+1}{n} r_{\mathrm{CO}}, \quad r_{\mathrm{C}_n\mathrm{H}_{2n+2}} = -\frac{1}{n} r_{\mathrm{CO}} \quad (4)$$

Please cite this article in press as: M.R. Kamali et al., A multi-component two-phase lattice Boltzmann method applied to a 1-D Fischer–Tropsch reactor, Chem. Eng. J. (2012), http://dx.doi.org/10.1016/j.cej.2012.07.019

where $[H_2]$ is the molar concentration of hydrogen and k_s [length/time] denotes the surface reaction constant.

3. Numerical method

This study exploits the LB approach in which each component or phase is represented by a set of fictitious particles rather than by the usual continuum variables. These fictitious particles, which are allowed to move on a regular lattice with their own discrete velocity distribution functions, carry the macroscopic properties such as density. These particles move (e.g., on the lattice type D_3Q_{19}) and collide with each other as hard spheres resulting in a redistribution in the velocity space such that total mass, momentum and energy in the system are conserved [4,21,31]. In the so-called BGK approximation), this redistribution is conceived as a relaxation to an equilibrium Maxwell distribution with a single relaxation time [32]. This relaxation time is an important parameter whose role of responding to spatial or temporal variations is equivalent to that of viscosity in the flow of fluids or of diffusion coefficients in species transport.

For the simulation of the transport processes and the chemical reactions involved in the Fischer–Tropsch reactions, the LB method has to be extended. The multi-component, multi-phase model due to Shan and Chen [5,8,17] is at the basis of this extension. With multiple components and phases, their mutual interaction has to be taken into account. In the LB conceptual framework, the interaction between fictitious particles representing the different components or phases is described in terms of the interaction potential functions ψ of the multiple components and a so-called coupling strength G_{ij}. The same is done with respect for the interaction between a component and a solid wall which is then governed by the coupling strength G_{iw}. This coupling strength affects the degree of miscibility and solubility of two components, the sharpness of a phase interface as well as the surface tension (in the case of a gas–liquid system), and the wettability of a solid surface (in the case of a gas/liquid/solid contact: see e.g., [33]).

In general, a positive G-value denotes repulsive forces, while a negative value represents mutual attraction. A value of zero for G_{ii} for component i mimics ideal gas behaviour. In a multi-component mixture, interaction potentials have to be selected for each individual component as well as between any two components. As an example, relevant to the topic of this paper: suppose we have a two-component system comprising a paraffin (component 1) and H_2 (component 2). To have paraffin condensed into the liquid phase, a negative G_{11}-value (attractive interaction) is attributed to the paraffin. As H_2 is nearly ideal, we postulate $G_{22} = 0$. Then, to obtain the desired solubility of H_2 in the paraffin, we tune the interaction between paraffin and H_2 by adjusting the value for G_{12}. Selecting proper values for all G_{ij}'s and G_{iw}'s to mimic the correct physical behaviour (solubilities, phase separation) is a tedious operation as these values also have a strong impact on the numerical stability of the calculations.

The potential function ψ depends on the local density and expresses the thermodynamic behaviour of a fluid commonly described in terms of an equation of state (EOS). The original idea in the Shan–Chen model was to use an arbitrary exponential function for the interaction potentials. One of the inherent limitations was the small range of the achievable density ratios between different phases or components. As shown by Yuan and Schaefer [18] and later on by Kupershtokh et al. [34], implementing any non-ideal EOS in the Shan–Chen force formulation makes it possible to attain at substantially higher values (beyond 1000 in single-component) for the phase density ratio [33]. In any non-ideal EOS, the reduced temperature – being the ratio between temperature and the critical temperature – is an important variable defining the properties of the liquid and vapour phase; in our LB simulations the reduced temperature is essentially a tuning variable to arrive at the desired density ratio in the mixture.

Shan and Doolen [19,20] showed that the evolution equation for each component in the Shan–Chen approach is simply the convection–diffusion equation for that particular component in the system. The diffusion coefficient of each component is dependent on its relaxation time and its interactions with other components. Since the kinematic viscosity of the fluid is also controlled by this relaxation time, this automatically implies the Schmidt number to be unity. This limitation can be overcome by employing a density dependent relaxation time for the solutes.

In the single-relaxation-time LB scheme, the relaxation time is normally assumed to be independent of mixture density. For a pure component system, the kinematic viscosity and the diffusion coefficient are then the same for the liquid and gas phases; by allowing the relaxation time to be a function of density, one can permit different kinematic viscosities and diffusivities for the gas and liquid phases. When the same relaxation time is employed for all the species in a mixture, the Schmidt number comes out to be unity for all the species in an ideal gas mixture and nearly so for non-ideal gas and liquid mixtures. The Schmidt number, however, is much larger than unity in liquids. Exercising independent control over the diffusivities and viscosity of a liquid mixture poses some challenges; liquid mixtures where the solutes are present at small concentrations, however, can be handled quite readily: the relaxation time of the *solvent* is chosen to get the desired liquid phase viscosity and treated as a constant independent of mixture density, while the relaxation times for the *solute* species are chosen to be a strong function of the mixture density – at low densities representative of vapour phase, they approach the same value as for the solvent and at high mixture densities they assume much smaller values. This density dependence of the relaxation time for the sparingly soluble solutes has only a weak effect on viscosity of the liquid, but allows slow *solute* diffusion (i.e., large Schmidt numbers *Sc*).

For instance, in a two-component system the relaxation time of the *solute* A, τ_A, as a function of the mixture density could be defined as Eq. (5), which is maximum in the gas phase, e.g. $\tau_A^G = \delta t$, and minimum in the liquid phase, e.g. $\tau_A^L = 0.5\delta t(1 + Sc^{-1})$, while linearly decreasing by shifting from gas to liquid in the diffused interface.

$$\tau_A(z,t) = \begin{cases} \tau_A^G & \rho \leqslant \rho_1 \\ \tau_A^G + (\tau_A^L - \tau_A^G)\frac{\rho-\rho_1}{\rho_2-\rho_1} & \rho_1 \leqslant \rho(z,t) \leqslant \rho_2 \\ \tau_A^L & \rho > \rho_2 \end{cases} \tag{5}$$

where $\rho_1 = 1.1\rho^G$ and $\rho_2 = 0.9\rho^L$, while ρ^G and ρ^L are the total gas and liquid phase densities.

Running successful LB simulations depends on selecting proper values for three types of typical LB variables: the potential functions ψ, the coupling strengths G_{ij}, and the relaxation time τ. This selection process is especially delicate when two-phase flow and multi-component mass transport have to be simulated.

4. Surface reaction implementation

Consider a 1-D Cartesian computational domain, one wall of which is the no-slip reactive surface, with the z-axis normal away the reactive wall. The two species A and B are involved in the surface reaction which is first order in A. On the wall ($z = z_w$) we thus have:

$$-D\nabla_z C(z_w) = k_s C(z_w) \tag{6}$$

Here D is the diffusion coefficient, k_s is the surface reaction constant and C is the mass concentration of species A. In our boundary condition implementation, the no-slip reactive surface is located

Please cite this article in press as: M.R. Kamali et al., A multi-component two-phase lattice Boltzmann method applied to a 1-D Fischer–Tropsch reactor, Chem. Eng. J. (2012), http://dx.doi.org/10.1016/j.cej.2012.07.019

halfway between two grid points. The first grid point inside the domain, seen from the reactive surface, is at $z_1 = z_w + \frac{1}{2}\delta z$, where δz is the grid spacing. To implement the surface reaction, we use a modified bounce-back rule. When a particle of type A hits the wall, fraction k_s^{LB} of its mass is converted into B, while the remaining fraction $1 - k_s^{LB}$ of its mass is conserved as A. Here k_s^{LB} is the dimensionless surface reaction constant. The reaction rate at the wall point is:

$$r = k_s^{LB}\phi \tag{7}$$

where ϕ is the z-component of the incoming mass flux of A onto the wall. This flux is emitted from z_1 and is defined as:

$$\phi = \sum_{\xi=1}^{18} h_\xi f_\xi(z_1)\left(\vec{e}_\xi \cdot \vec{e}_z\right) \tag{8}$$

In this equation, ξ is an index that denotes a discrete LB velocity direction ($\vec{e}_\xi$) and $f_\xi(z_1)$ is the velocity distribution function for that direction. For the particles moving towards the wall the function: $h_\xi = 1$ and $\vec{e}_\xi \cdot \vec{e}_z = -\delta z/\delta t$. For the particles moving away from the wall $h_\xi = 0$ and $\vec{e}_\xi \cdot \vec{e}_z = \delta z/\delta t$. In order to evaluate Eq. (8), we assume that the flow is in equilibrium: $f_\xi(z_1) = f_\xi^{eq}(z_1)$ and that the macroscopic velocity is zero: $\vec{u}(z_1) = \vec{0}$, such that $f_\xi^{eq}(z_1) = w_\xi C(z_1)$, where w_ξ is the lattice weighing factor for direction ξ. Using these approximations in the D_3Q_{19} lattice topology leads to: $\sum_{\xi=1}^{18} h_\xi w_\xi = \frac{1}{6}$, which can then define the mass flux (Eq. (8)) as follows:

$$\phi = \frac{C(z_1)}{6}\frac{\delta z}{\delta t} \tag{9}$$

To relate the real reaction rate constant k_s, defined in Eq. (6), to the dimensionless LB reaction rate constant k_s^{LB}, we impose that the reaction rate: $r = k_s^{LB}\phi$ is equivalent to $r = k_s C(z_w)$:

$$\frac{1}{6}\frac{\delta z}{\delta t}k_s^{LB}C(z_1) = k_s C(z_w) \tag{10}$$

$C(z_1)$ could be expressed in terms of $C(z_w)$ by using a Taylor expansion:

$$C(z_1) = C(z_w) + \frac{\delta z}{2}\nabla_z C(z_w) \tag{11}$$

and by using Eq. (6), to express $\nabla_z C(z_w)$ in terms of $C(z_w)$, one finds the following expression for the LB reaction constant.

$$k_s^{LB} = \left(\frac{6k_s\delta t}{\delta z}\right)\Big/\left(1 + \frac{k_s\delta z}{2D}\right) \tag{12}$$

5. Validation for a 1st order single-phase surface reaction

The LB model developed is first validated for a one-dimensional single-phase reaction–diffusion example where a first-order surface reaction takes place on the bounding walls. The result of the LB simulation is compared with the analytical solution to the problem. In this case, a stagnant gas A next to a reactive surface is converted into a second gaseous species B with the same molecular mass. The initial mass fraction of species A $x_A(z, t = 0) = 1$ everywhere in the computational domain. Product B is only produced after the reaction is initiated. The analytical solution to this *batch process* for short times ($Fo \ll 1$, where the Fourier number $Fo = Dt/L^2$) is:

$$\frac{x_A(\tilde{z},\tilde{t})}{x_A(\tilde{z},0)} = \frac{C(\tilde{z},\tilde{t})}{C(\tilde{z},0)} = erf\left(\frac{\tilde{z}}{2\sqrt{\tilde{t}}}\right) + e^{(\tilde{z}+\tilde{t})}erfc\left(\frac{\tilde{z}}{2\sqrt{\tilde{t}}}\right) \tag{13}$$

where $\tilde{z} = zk_s/D$ and $\tilde{t} = tk_s^2/D$ are the characteristic space and time.

The Damköhler number ($Da_s = Lk_s/D$, where L is the computational domain size) in the example described below in Fig. 1 is as high as 4000, and one can readily anticipate appreciable diffusion limitation. The simulation results are compared with the analytical solution at different Fo-values. In our initial simulation, the 1-D computational domain was discretized into 256 grid points; later on, the number of grid points was varied. This domain is bounded by two walls, located halfway between grid points 1 and 2 and halfway between grid points 255 and 256. As stated before the comparison can be made only for small Fo-values.

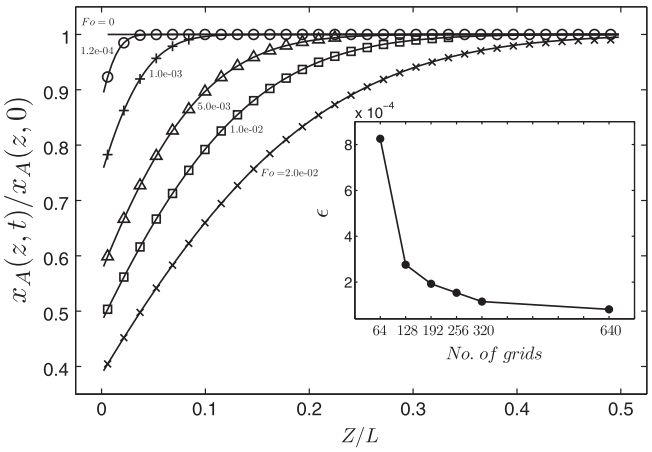

Fig. 1. Validation of LB model against analytical solution for a one-dimensional single-phase reaction–diffusion problem. First-order surface reaction at catalytic wall ($z = 0$ is shown); $Da_s = 4000$. Bullets: LB simulation. Lines: analytical solution at various Fourier numbers. Inset: Results from a grid dependency study with the spatially and Fo-averaged relative error $\varepsilon = |x^{LB} - x^{an.}|/x^{an.}$.

In Fig. 1, $x_A(z, t)/x_A(z, 0)$ is plotted vs. z/L for various Fo values. The LB simulation results are represented by markers and compared against the analytical solutions shown with lines. In this figure, $z/L = 0$ is the position of the reactive wall and $z/L = 0.5$ is halfway the computational domain. The solution to this problem is symmetric with respect to the domain centre. It is clear that the LB simulation result is in good agreement with the analytical solution. The relative error between our LB simulation results and the analytical solution, defined by $\varepsilon = |x^{LB} - x^{an.}|/x^{an.}$, is a measure of the accuracy of the solution obtained. In order to arrive at a single error value for each grid resolution which reflects both temporal and spatial variations, the errors were first averaged over space and next over non-dimensional time or Fo number in the range of validity of the analytical solution ($Fo < 0.02$). The accuracy of the LB model is further assessed by refining the grid. In this study, we kept Da_s constant and evaluated the error at identical Fo values but different grid sizes. The time and space averaged relative errors are shown as a function of the dimensionless grid size in the inset of Fig. 1. The relative error is already very small even at $\delta z/L = 1/64$; increasing the number of grids by a factor of ten reduces the error further. Analogous validation of the model for different Damköhler numbers gave equally accurate results.

6. Validation for a first-order surface reaction behind a growing liquid film

The second validation case is also a first-order reaction $A \xrightarrow{k_s} B$ taking place at the two boundaries of a channel as in the previous example; now, A is an ideal gas and B obeys the Redlich–Kwong EOS [18]. The reduced temperature T_R (=T/T_c, with T_c the critical temperature) used in the EOS for B was set to $T_R = 0.7$ – resulting in liquid and gas densities of $\rho^L = 7.6$ and $\rho^G = 0.26$ (in lattice units), respectively. Under such conditions, the product B is predominantly in the liquid phase; so, as the reaction proceeds, the thickness of the liquid film grows. The geometry of the problem is sketched in Fig. 2 in which j denotes the reactant component A. This simple idealisation of the FTS reaction of current interest, where gaseous reactants

Please cite this article in press as: M.R. Kamali et al., A multi-component two-phase lattice Boltzmann method applied to a 1-D Fischer–Tropsch reactor, Chem. Eng. J. (2012), http://dx.doi.org/10.1016/j.cej.2012.07.019

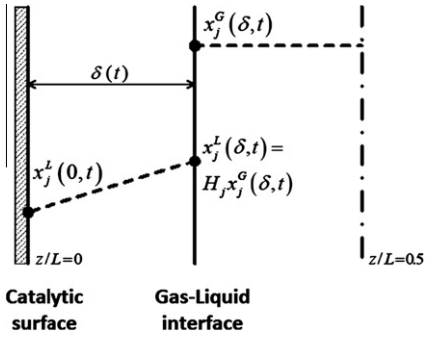

Fig. 2. schematic representation of the liquid film growth due to surface reaction (j: component).

Table 1
Parameters used in the simulation of liquid film growth due to first order surface reaction; and the obtained densities and Henry's constant before the reaction starts (w: wall, A: ideal gas-like reactant, B: RK liquid-like product).

T_R	$G_{BB}=G_{Bw}$	$G_{AA}=G_{Aw}$	G_{AB}	ρ^L	ρ^G	ρ^L/ρ^G	H_A
0.7	−1	0	0	7.6	0.26	29.23	8.26e−4

lead to a liquid-forming product, permits an analytical solution for the film growth, which can be used to validate the LB approach. In this sample study, the *Sc* number is unity.

In this example, the Shan–Chen multi-component approach was used to handle this two-component mixture in two phases, which requires specification of species–species (G_{ij}) and species–wall (G_{iw}) interaction parameters. Table 1 shows the set of parameters used in this study. In this table, Henry's constant is $H_A = x_A^L(\delta,t)/x_A^G(\delta,t)$ where $x_A^L(\delta,t)$ and $x_A^G(\delta,t)$ denote mass fractions of component A at the liquid and gas sides of an equilibrium interface.

Unlike the previous example, the LB simulations begin with an initial condition where a layer of liquid is present on both catalyst walls $\delta_0/L = 9.64\times10^{-4}$. The vapour and liquid regions were first allowed to equilibrate under *non-reacting* conditions. At time $t = 0$, A starts reacting on the catalytic surface; it is converted into B which contributes to liquid film growth. In our simulations, the computational domain size (L) was chosen to be very much larger than the initial film thickness ($\delta_0/L \to 0$). One can readily argue that – when the film Damköhler number ($Da_s^\delta = k_s\delta/D$) is much smaller than $1/H_A x_A^G(\delta,t)$, and the supply of reactant A in the vapour phase is large (achieved by keeping the $1-\delta/L$ close to unity) – a quasi-steady state description (diffusion keeps up with the reaction) is sufficiently accurate, permitting the analytical solution:

$$\bar{x}_B^L \frac{d\delta}{dt} = \frac{k_s x_A^L(\delta,t)}{1+k_s\delta/D} = \frac{k_s H_A x_A^G(\delta,t)}{1+k_s\delta/D} \tag{14}$$

Here, $\bar{x}_B^L(z<\delta,t)$ is the average mass fraction of the product component B in the liquid (very close to unity) and $x_A^G(\delta,t)$ is the mass fraction of A at the vapour–liquid interface (essentially constant at early times, given the large excess of vapour phase). Eq. (14) can be integrated which leads to the film growth formulation with respect to time t.

$$\frac{\delta(t)-\delta_0}{L} + \frac{1}{2}Da_s\frac{\delta^2(t)-\delta_0^2}{L^2} = Da_s H_A \frac{x_A^G(\delta,t)}{\bar{x}_B} Fo \tag{15}$$

Without the simplification of the quasi-steady state, *i.e.* acknowledging that starting from the equilibrium the concentration profile gradually changes due to the diffusion controlled chemical reaction at the surface, the transient diffusion equation has to be solved with the above boundary conditions. With a mass fraction profile (in the liquid) of the shape

$$x_A^L(z,t) = x_A^L(\delta,t) + x_A^L(\delta,t)(z-\delta)g(z,t) \tag{16}$$

after proper scaling

$$\tilde{x}_A^L = \frac{x_A^L(z,t)}{x_A^L(\delta,t)};\quad \tilde{z} = \frac{k_s z}{D} = Da_s^z;\quad \tilde{\delta} = \frac{k_s\delta}{D} = Da_s^\delta;\quad \tilde{t} = \frac{k_s^2 t}{D} \tag{17}$$

and with the trial function $g(\tilde{z},\tilde{t}) = -\tilde{t} + G(\tilde{z})$ a regular perturbation analysis for $\frac{x_A^L(\delta,t)}{x_B^L(z,t)} \ll 1$ (suggested by Tien [35]) yields

$$\tilde{x}_A^L = 1 + \tilde{z} + \frac{x_A^L(\delta,t)}{x_B^L(z,t)}\left\{-\tilde{t} - \tilde{z}\left(\tilde{t} + \frac{\tilde{z}}{2} + \frac{\tilde{z}^2}{6}\right)\right\} + \cdots \tag{18}$$

$$\tilde{\delta} = \tilde{\delta}_0 + \frac{x_A^L(\delta,t)}{x_B^L(z,t)}\tilde{t} - \left(\frac{x_A^L(\delta,t)}{x_B^L(z,t)}\right)^2\frac{\tilde{t}^2}{2} + \cdots \tag{19}$$

Two different approaches, potentially leading to identical results, were used for calculating the interface position for LB simulations. In the first approach, the interface was calculated by

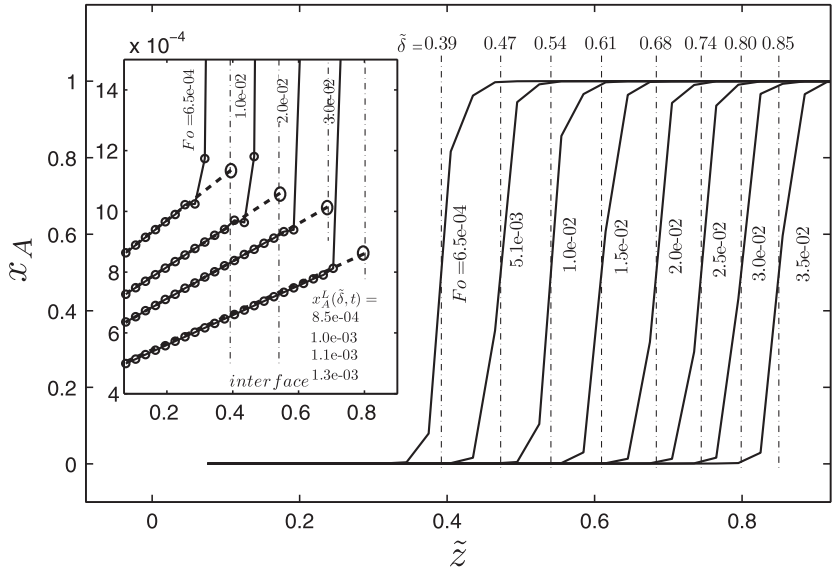

Fig. 3. Mass fraction of reactant A next to the catalytic surface at different *Fo* values. Broken lines indicate the interface locations at various *Fo*. Inset: the mass fraction linear profiles in the liquid phase and the predicted mass fraction at the interface, at various *Fo* numbers.

Please cite this article in press as: M.R. Kamali et al., A multi-component two-phase lattice Boltzmann method applied to a 1-D Fischer–Tropsch reactor, Chem. Eng. J. (2012), http://dx.doi.org/10.1016/j.cej.2012.07.019

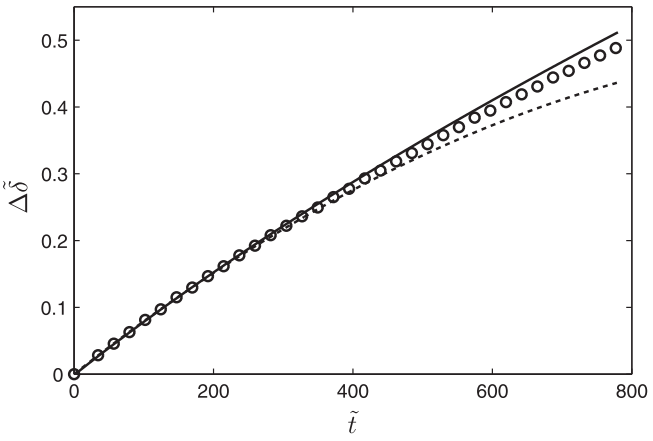

Fig. 4. Comparison of film growth from LB (open circles) with the two analytical models of Eq. (15) (solid line) and Eq. (19) (broken line), for $Da_s = 288$, $H_A = 8.3e{-}4$, $\tilde{\delta}_0 = k_s\delta_0/L = 4.82e{-}6$, $x_A^G(\tilde{z}, \tilde{t} = 0) = 1$.

finding the maximum in the gradient of the density field – being equivalent to positioning the sharp interface at 50% liquid. The second approach was by tracking the total mass of the liquid-like component in the whole system which is composed of the liquid and gas regions.

Fig. 3 presents the mass fraction distribution of reactant A very close to the reacting surface vs. characteristic distance from the wall $\tilde{z} = k_s z/D$ at different *Fo*-values as predicted by the LB code. This figure also shows the interface position (shown by vertical broken lines) at various *Fo*-values. In the inset of Fig. 3, the mass fraction of component A next to the wall is shown in greater detail. The linear profile of reactant is clearly seen in this picture – providing sufficient evidence for the assumptions we pursued in both analytical solutions. This linear profile is the result of high diffusion rate compared to the surface reaction rate in the thin liquid film. The intersection of this linear line with the interface provides the mass fraction at the interface. Fig. 4 shows the comparison between the characteristic film thicknesses $\tilde{\delta}(\tilde{t}) = k_s\delta(t)/D$ as obtained from LB simulation and as predicted by Eqs. (15) and (19). It is clear from this figure, that the LB predicts the film thickness pretty well at early times. However, in the later times of the reaction, Henry's constant and the reactant concentration on the interface change which do not satisfy the assumptions of the analytical solutions. This can create some discrepancies between LB simulation results and the analytical solutions at very late stages of time.

7. The FTS reaction with the LB method

7.1. Problem description: 1-D simulation of the FTS reaction

The LB model developed was used for the one-dimensional simulation of the FTS reaction based on the kinetic model due to Post et al. (Eq. (4)). The computational domain, namely, the region between two parallel catalytic walls, is discretized using 640 grid points along the *z*-direction (pointing normal to the walls). The geometry of the problem of interest is similar to that of Fig. 2. The *j* in this figure is representative of the components CO and H_2 or reactants. The internal mass transfer limitations of a real-world porous catalyst due to diffusion or back-diffusion through the tortuous channels in the catalyst particles are not considered here; instead, a flat catalytic surface is studied. The surface reaction kinetics is implemented at the wall nodes as described before in Eqs. (6)–(12) by the modified bounce-back rule.

While Post et al. present their kinetics model in terms of molar based quantities, the LB algorithm is based on mass concentrations. The reaction rates in the Post et al. model can readily be converted to mass-based rates:

$$r_{CO}^{LB}(z,t) = -\left(\frac{m_{CO}}{m_{H_2}}\right) k_s^{LB} \phi_{H_2}(z,t) \tag{20}$$

$$r_{H_2}^{LB}(z,t) = \left(\frac{m_{H_2}}{m_{CO}}\right)\left(\frac{2n+1}{n}\right) r_{CO}^{LB}(z,t)$$

$$r_{C_nH_{2n+2}}^{LB}(z,t) = -\left(\frac{m_{C_nH_{2n+2}}}{m_{CO}}\right)\left(\frac{1}{n}\right) r_{CO}^{LB}(z,t)$$

$$r_{H_2O}^{LB}(z,t) = \left(\frac{m_{H_2O}}{m_{CO}}\right) r_{CO}^{LB}(z,t)$$

Here, $\phi_{H_2}(z,t)$ is the *z*-component of the incoming mass flux of H_2 onto the wall and is defined as in Eq. (8).

Since the reaction kinetics is first order in H_2, one can still use Eq. (12) to convert the dimensionless k_s^{LB} to the real reaction constant k_s and vice versa. The reaction being first order in H_2 allows us to calculate the paraffinic film thickness growth through Eqs. (15) and (19). To this purpose, k_s should be the reaction constant based on the consumption of H_2. By using proper conversion in the mass based stoichiometric reaction of Eq. (20), the H_2 based k_s value will be:

$$k_s = \left(\frac{m_{C_nH_{2n+2}}}{m_{H_2}}\right)\left(\frac{1}{2n+1}\right)\left(\frac{2Dk_s^{LB}\delta z}{12D\delta t - k_s^{LB}(\delta z)^2}\right) \tag{21}$$

The k_s value calculated from this equation is the basis for all figures in the FTS results section. In our simulations, the Damköhler number with respect to H_2 is 0.56.

In this illustrative FTS example, just one typical paraffinic product was considered for the sake of simplicity. As a result, only four components are involved in the reaction, *viz.* CO, H_2, H_2O, and a typical paraffinic compound C_nH_{2n+2}. The paraffin follows the Redlich–Kwong EOS [18], while the other three species are considered to be ideal gases, just like in the FTS under the usual operating conditions.

The Shan–Chen multi-component approach was used to handle this four-component mixture in two phases, which requires specification of species–species (G_{ij}) and species–wall (G_{iw}) interaction parameters. The interaction parameters G_{ij} (*i* = paraffin; *j* = CO, H_2, H_2O) were chosen to be positive (indicative of repulsion), which allowed us to tune the solubility of the gas-like components in a paraffinic liquid phase. Table 2 provides the details of the parameters used together with the resulting densities of the liquid and gas phases, and Henry's constants before the reaction starts. Henry's constants in this table are calculated on the basis of the assumption that the interaction potential functions of the gas-like components depend on density according to $\psi_j = \sqrt{\rho_j}(j = CO, H_2, H_2O)$.

The simulation begins with a thin layer ($\delta_0/L = 0.032$) of paraffin liquid ($n = 15$), *in equilibrium* with H_2, CO and H_2O in the vapour phase. The computational domain is large compared to the liquid film thickness to make sure H_2 and CO are abundantly available in the system. The initial amount of H_2O in the system is chosen to be very low. After the reaction has been initiated, the liquid film

Table 2
Parameters used in the simulation of FTS reaction, densities (in lattice units), and Henry's constants before the reaction starts; *w*: wall, *i*: paraffinic RK liquid-like species, *j*: CO, H_2,H_2O (ideal gas-like species).

T_R	$G_{ii} = G_{iw}$	$G_{jj} = G_{jw}$	$G_{ij} = G_{ji}$	ρ^L	ρ^G	ρ^L/ρ^G	H_j
0.7	−1	0	1e−3	7.7	0.3	25.7	*j* = CO: 7.33e−4 H_2: 1.95e−2 H_2O: 4.61e−2

grows gradually as a result of the formation of the paraffin. The continuous process of diffusion of CO and H_2 towards the catalyst surface and the back-diffusion of water vapour towards the liquid–gas interface, and the growth of the liquid film itself are evolved via the LB scheme.

As mentioned earlier, the product in the liquid layer tracked in our simulation is a typical paraffinic compound with n carbon atoms which is representative of the possible carbon chain distribution that ranges from C_1 to C_{15}. For this single representative paraffin, the pertinent carbon chain distribution is calculated by means of the ASF model mentioned before. In our simulations this calculation is performed in a post-processing step at the end of the simulation: given the amount of the C_n formed and the value of the chain distribution probability α, the ASF distribution – see Eqs. (2) and (3) – may provide the yield of the various paraffins. According to the experimental data of De Deugd [36] and curve fittings for various α by Vervloet et al. [25], the values of κ_α and β in Eq. (1) could be chosen as 0.057 and 1.76, respectively.

In principle, this post-processing step might be carried out at several moments in time during the simulation. While in our simulations the system is isothermal with closed boundaries and the catalyst does not change, the syngas ratio continually changes as the result of the gradual conversion of reactants via the reaction. A varying syngas ratio results in a α and the mass and mole fractions of the various paraffins varying in time.

7.2. Results and discussion: One-dimensional simulation of the FTS reaction

The implementation of the above 1-D FTS model leads to multiple results which could be helpful in understanding certain aspects of the FTS better. We will start by showing the snapshots of the spatial distribution of the various mole fractions adjacent to the catalyst surface in Fig. 5. In this plot $\tilde{t}$ is the characteristic time being defined as $\tilde{t} = k_s^2 t/D = (k_s L/D)^2 (tD/L^2) = Da_s^2 Fo$ where D is the diffusion coefficient $(0.167(\delta x)^2/\delta t)$ and k_s is the surface reaction constant with respect to the H_2 which is calculated from Eq. (21). First, this figure illustrates that – as mentioned before – the LB method is a diffusive method. The bullets on the paraffin curve show that the interface spans 3–4 grid points. The position of the interface may be attributed to the point where the gradient in the density or concentration of the liquid component is maximum.

Fig. 5 shows that at $\tilde{t} = 0$, denoting the moment in time the surface reaction is initiated, a thin layer of dimensionless thickness δ_0/L = 0.032 is covering the catalyst surface, in equilibrium with the other three components. The equilibrium states for these three gaseous components (H_2, CO, H_2O) are imposed through the relaxation time and the interaction coefficients which satisfy their mutual diffusivities and Henry's constant. Fig. 5 further shows that at $\tilde{t} = 0$ the H_2/CO molar ratio is around 1.8 (see also Figs. 8 and 9) and the initial water mole fraction is almost zero. To be more precise: the equilibrated mole fractions in the film next to the wall z/L = 0 at $\tilde{t} = 0$ are $\chi^s_{H_2} = 11.4\text{e-}2$, $\chi^s_{CO} = 0.28\text{e-}2$, $\chi^s_{C_nH_{2n+2}} = 88.2\text{e-}2$, and $\chi^s_{H_2O} = 0.16\text{e-}2$.

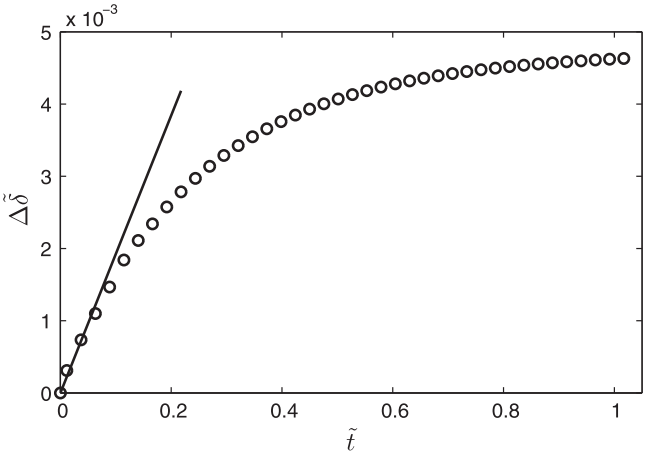

Fig. 6. Paraffin film growth obtained from LB simulation (circles) compared to the quasi-steady model of Eq. (15) (solid line); Da_s = 0.56, $H_{H_2} = 1.95\text{e-}2$, $\tilde{\delta}_0 = k_s\delta_0/L = 4.69\text{e-}6$, $\Delta\tilde{\delta} = \tilde{\delta} - \tilde{\delta}_0$.

The initial film is considered to be very thin and the Damköhler number is taken small enough to give sufficient time for the gaseous reactants to diffuse through the liquid layer and the gaseous product (H_2O) to diffuse back towards the interface. As a result, the system is diffusion dominated and a linear profile for the mole fractions of the reactants inside the film are accomplished. The snapshots further show how the paraffin film grows in time and how the mole fractions of the four components involved in the reaction change. The mole fraction of the paraffin component in the gas phase is almost zero. The equation of state and the reduced temperature together with the interaction coefficients maintain these properties. As a result, the paraffin production due to surface reaction almost exclusively contributes to film growth.

Fig. 6, shows the comparison of characteristic film thickness $\tilde{\delta}(\tilde{t})$ calculated by the LB method (circles) with the one calculated from the quasi-steady state theory of Eq. (15). This comparison shows a

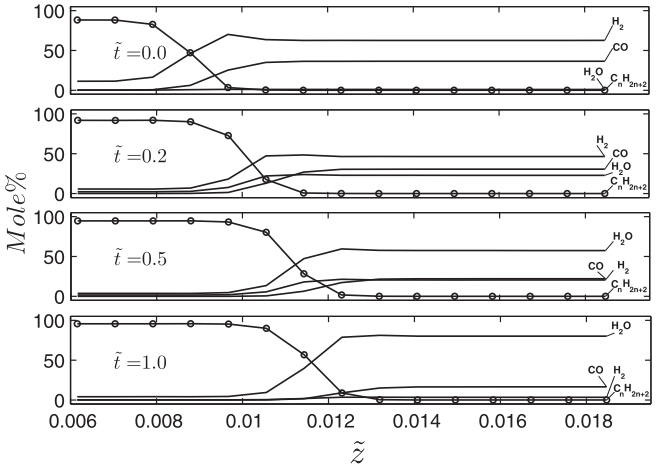

Fig. 5. Molar percent distribution of the four species vs. characteristic length $\tilde{\delta}_0 = k_s\delta_0/L = 4.69\text{e-}6$ at different characteristic time $\tilde{t} = k_s^2 t/D$.

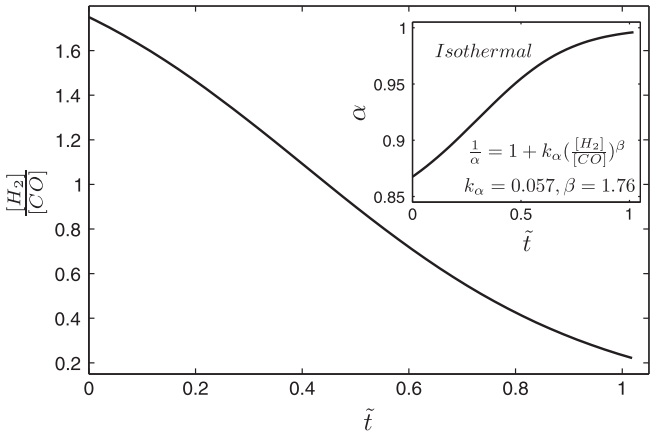

Fig. 7. Decrease of syngas ratio at the wall during the isothermal reaction. Inset: the increase in carbon growth probability during the reaction.

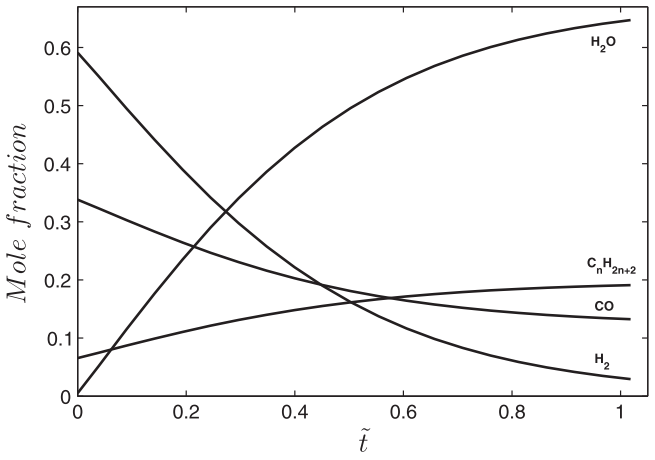

Fig. 8. Mole fractions of the four components involved in the FTS reaction vs. characteristic time.

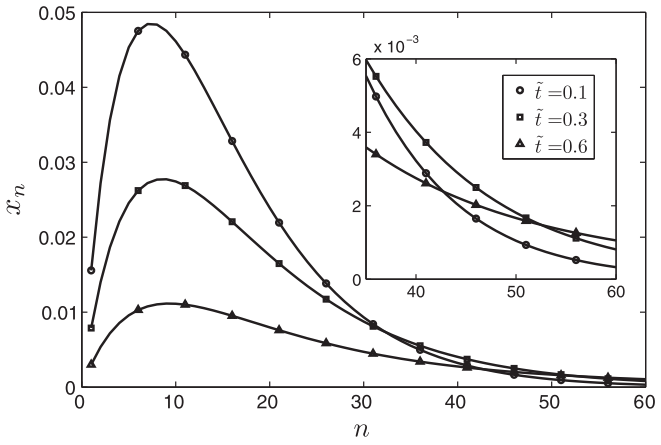

Fig. 10. Paraffin product distribution in time for the carbon chains of C_1–C_{60}; inset: zoom in the higher carbon chains.

good agreement in the early times of the reaction in which the Henry's constant and the species concentration on the interface do not significantly deviate from their initial values. By any means, this plot validates the reaction constant k_s calculated from Eq. (21).

The syngas ratio at the wall is one of the most important variables affecting the FTS, particularly the product distribution. Fig. 7 shows how the syngas ratio varies with the characteristic time $\tilde{t} = 0$. The corresponding chain growth probability α in this isothermal model is shown in the inset of Fig. 7. The reactive mixture being stoichiometric, the H_2/CO ratio starts from around 1.8 at $\tilde{t} = 0$ and drops to 0.2 at $\tilde{t} = 1$ as a result of the faster diffusion of hydrogen. After this time, the rate is virtually zero resulting in a zero film growth rate.

The development of the mole fractions (averaged over the domain/film) of the four species involved in the reaction over time is shown in Fig. 8. Due to the value 0.56 of the Damköhler number (based on k_s for H_2), hydrocarbon production rate and consequently film growth rate are very slow and keep the macroscopic velocities and therefore the convective mass fluxes negligible.

As mentioned before, the kinetic model due to Post et al. is valid up to a CO conversion of 60%. Fig. 8 shows that in our simulation the validity of the kinetic model sustains almost till the end ($\tilde{t} = 1$) which corresponds to the period that the CO mole fraction declines from initial value of 0.34 to 0.14. The total hydrocarbon C_nH_{2n+2} production as a function of characteristic time (from Fig. 8) can be combined with the transient chain growth probability information in Fig. 7 to find the paraffin product break-up in terms of C_1, C_2, C_3, C_4 and C_{5+} as shown in Fig. 9.

Hydrocarbon selectivity of the catalytic system may depend on carbon chain growth probability. An increase in α reflects a decay in the C_1–C_4 concentrations and a simultaneous increase in the heavier hydrocarbons concentrations, as illustrated by Fig. 9. At the end of the process, mostly heavier hydrocarbons may be formed – on the proviso that the Post et al. kinetics is still valid. This could be clearly seen from Fig. 10 which shows the mass fraction product distribution variation over time. Fig. 10 further shows that the mass-based average of the product distribution is around C_{15} and this value hardly changes over time – which was an *ab initio* assumption in the simulation.

Results like this increase our quantitative understanding of the FTS reactions. Of course, quite a few steps have to be made before such simulations will become representative of the real FTS reaction – under relevant operating conditions – such as the use of different relaxation times for the various components, the introduction of the thermal energy balance equation, the introduction of more complex chemistry, and the extension to (more) realistic 3-D geometries. We believe that this paper is an important step towards a better description and understanding of the complex FTS (or similar) reactions.

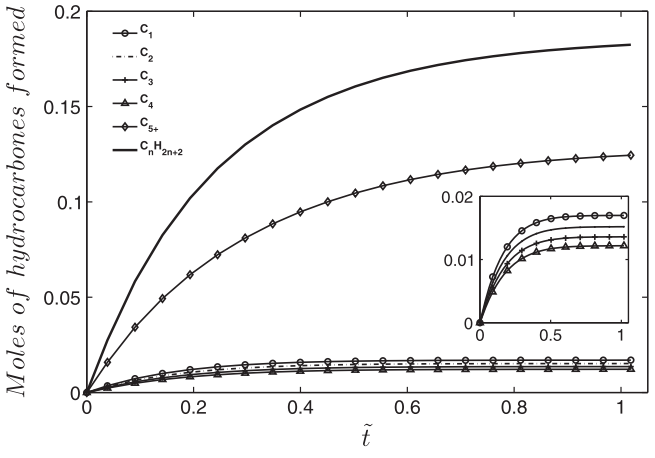

Fig. 9. The various paraffinic products vs. characteristic time.

8. Conclusion

A lattice Boltzmann based technique was presented which was capable of computationally reproducing a 1-D simplification of multi-component two-phase surface reaction representative of a two-phase catalytic chemical reactor. The surface reaction implementation has been validated against analytical models for a system with first-order kinetics in both a single-phase and a two-phase canonical case. The surface reaction constant used in the so-called modified bounce back rule is a dimensionless variable related to the surface reaction coefficient of interest and reflects the mass flux balance between the various species to and from the surface. The error of the method may be in the order of 0.01% compared to the analytical solutions in the two canonical cases. The complex interplay of diffusion and surface reaction accompanied with phase change in a multi-component two-phase system could be successfully handled with this lattice Boltzmann method. We illustrated this by conducting a simulation of a simplified 1-D isothermal Fischer–Tropsch Synthesis. Relevant information was deduced as to transients in the syngas molar ratio, film thickness,

Please cite this article in press as: M.R. Kamali et al., A multi-component two-phase lattice Boltzmann method applied to a 1-D Fischer–Tropsch reactor, Chem. Eng. J. (2012), http://dx.doi.org/10.1016/j.cej.2012.07.019

selectivity and product distribution during the course of the reaction. This paper sets the scene for a more realistic simulation of the FTS reactions through future improvements in the LB handling of species transport and chemical reactions, through inclusion of heat transport, flow, and better chemistry, and owing to expansion into more realistic 3-D geometries.

Acknowledgment

This research is supported by the Dutch Technology Foundation STW, the Applied Science Division of the Netherlands Organization for Scientific Research (NWO).

References

[1] J. Zhang, Lattice Boltzmann method for microfluidics: models and applications, Microfluid. Nanofluid. 10 (2011) 1–28.
[2] H.E.A. Van den Akker, The Details of Turbulent Mixing Process and their Simulation, Adv. Chem. Eng. (2006) 151–229.
[3] J.J.J. Gillissen, H.E.A. Van den Akker, Direct numerical simulation of the turbulent flow in a baffled tank driven by a Rushton turbine, AIChE J. (2012).
[4] J. Derksen, H.E.A. Van Den Akker, Large eddy simulations on the flow driven by a Rushton turbine, AIChE J. 45 (1999) 209–221.
[5] K. Sankaranarayanan, X. Shan, I.G. Kevrekidis, S. Sundaresan, Analysis of drag and virtual mass forces in bubbly suspensions using an implicit formulation of the lattice Boltzmann method, J. Fluid Mech. 452 (2002) 61–96.
[6] J.J. Derksen, S. Sundaresan, Direct numerical simulations of dense suspensions: wave instabilities in liquid-fluidized beds, J. Fluid Mech. 587 (2007) 303–336.
[7] J.J.J. Gillissen, S. Sundaresan, H.E.A. Van Den Akker, A lattice Boltzmann study on the drag force in bubble swarms, J. Fluid Mech. 679 (2011) 101–121.
[8] X. Shan, H. Chen, Lattice Boltzmann model for simulating flows with multiple phases and components, Phys. Rev. E 47 (1993) 1815–1819.
[9] R.G.M. Van Der Sman, Galilean invariant lattice Boltzmann scheme for natural convection on square and rectangular lattices, Phys. Rev. E: Stat., Nonlinear, Soft Matter Phys. 74 (2006) (Art. No. 026705).
[10] G. De Prisco, X. Shan, Mass transport/diffusion and surface reaction process with lattice Boltzmann, Commun. Comput. Phys. 9 (2011) 1362–1374.
[11] S. Succi, G. Smith, E. Kaxiras, Lattice Boltzmann simulation of reactive microflows over catalytic surfaces, J. Stat. Phys. 107 (2002) 343–366.
[12] R. Verberg, A.J.C. Ladd, Simulation of chemical erosion in rough fractures, Phys. Rev. E: Stat., Nonlinear, Soft Matter Phys. 65 (2002). 056311/056311–056311/056316 (Art. No. 056311).
[13] Q. Kang, D. Zhang, S. Chen, X. He, Lattice Boltzmann simulation of chemical dissolution in porous media, Phys. Rev. E: Stat., Nonlinear, Soft Matter Phys. 65 (2002) (Art. No. 36318).
[14] D. Vervloet, M.R. Kamali, J.J.J. Gillissen, J. Nijenhuis, H.E.A. van den Akker, F. Kapteijn, J.R. van Ommen, Intensification of co-current gas–liquid reactors using structured catalytic packings: a multiscale approach, Catal. Today 147 (2009) S138–S143.
[15] T. Lee, P.F. Fischer, Eliminating parasitic currents in the lattice Boltzmann equation method for nonideal gases, Phys. Rev. E: Stat., Nonlinear, Soft Matter Phys. 74 (2006) (Art. No. 046709).
[16] Z. Guo, B. Shi, C. Zheng, Chequerboard effects on spurious currents in the lattice Boltzmann equation for two-phaseflows, Philos. Trans. R. Soc. A: Math., Phys. Eng. Sci. 369 (2011) 2283–2291.
[17] X. Shan, Analysis and reduction of the spurious current in a class of multiphase lattice Boltzmann models, Phys. Rev. E: Stat., Nonlinear, Soft Matter Phys. 73 (2006) (Art. No. 047701).
[18] P. Yuan, L. Schaefer, Equations of state in a lattice Boltzmann model, Phys. Fluids 18 (2006) (Art. No. 042101).
[19] X. Shan, G. Doolen, Multicomponent lattice-Boltzmann model with interparticle interaction, J. Stat. Phys. 81 (1995) 379–393.
[20] X. Shan, G. Doolen, Diffusion in a multicomponent lattice Boltzmann equation model, Phys. Rev. E – Stat. Phys., Plasmas, Fluids, Relat. Interdiscip. Topics 54 (1996) 3614–3620.
[21] S. Succi, The Lattice Boltzmann Equation for Fluid Dynamics and Beyond (Numerical Mathematics and Scientific Computation), 2001, Oxford University Press. ISBN: 0-19-850398-9
[22] S.D.C. Walsh, M.O. Saar, Interpolated lattice Boltzmann boundary conditions for surface reaction kinetics, Phys. Rev. E: Stat., Nonlinear, Soft Matter Phys. 82 (2010) (Art. No. 066703).
[23] G.P. Van Der Laan, A.A.C.M. Beenackers, Kinetics and selectivity of the Fischer–Tropsch synthesis: a literature review, Catal. Rev. – Sci. Eng. 41 (1999) 255–318.
[24] K. Pangarkar, Solving the Heat Transport Issue in Multiphase Fixed Bed Reactors, PhD Thesis, Applied Sciences, Delft University of Technology, Delft, 2010.
[25] D. Vervloet, F. Kapteijn, J. Nijenhuis, J.R. van Ommen, Fischer–Tropsch reaction–diffusion in a cobalt catalyst particle: aspects of activity and selectivity for a variable chain growth probability, Catal. Sci. Technol. 2 (6) (2012) 1221–1233.
[26] W.H. Zimmerman, J.A. Rossin, D.B. Bukur, Effect of particle size on the activity of a fused iron Fischer–Tropsch catalyst, Ind. Eng. Chem. Res.® 28 (1989) 406–413.
[27] M.F.M. Post, A.C. van't Hoog, J.K. Minderhoud, S.T. Sie, Diffusion limitations in Fischer–Tropsch catalysts, AIChE J. 35 (1989) 1107–1114.
[28] R. Krishna, S.T. Sie, Design and scale-up of the Fischer–Tropsch bubble column slurry reactor, Fuel Process. Technol. 64 (2000) 73–105.
[29] R. Guettel, T. Turek, Comparison of different reactor types for low temperature Fischer–Tropsch synthesis: a simulation study, Chem. Eng. Sci. 64 (2009) 955–964.
[30] I.C. Yates, C.N. Satterfield, Intrinsic kinetics of the Fischer–Tropsch synthesis on a cobalt catalyst, Energy Fuels 5 (1991) 168–173.
[31] D.A. Wolf-Gladrow, Lattice-Gas Cellular Automata and Lattice Boltzmann Models: An Introduction, Springer, 2000.
[32] P.L. Bhatnagar, E.P. Gross, M. Krook, A model for collision processes in gases. I. Small amplitude processes in charged and neutral one-component systems, Phys. Rev. 94 (1954) 511–525.
[33] M.R. Kamali, J.J.J. Gillissen, S. Sundaresan, H.E.A. Van den Akker, Contact line motion without slip in lattice Boltzmann simulations, Chem. Eng. Sci. 66 (2011) 3452–3458.
[34] A.L. Kupershtokh, D.A. Medvedev, D.I. Karpov, On equations of state in a lattice Boltzmann method, Comput. Math. Appl. 58 (2009) 965–974.
[35] J. Tien, Personal communication, 2012.
[36] R.M. De Deugd, Fischer–Tropsch Synthesis Revisited, PhD Thesis, Delft University of Technology, 2004.